Title

Cryogenic Stress-Driven Grain Growth Observed via Microcompression with in situ Electron Backscatter Diffraction

Journal

JOM, 72(5)

ISSN

1047-4838

Authors

Frazer, D
Bair, JL
Homer, ER
et al.

Publication Date

2020-05-01

DOI

10.1007/s11837-020-04075-x

Peer reviewed

Cryogenic stress-driven grain growth observed via microcompression with in-situ electron backscatter diffraction

D. Frazer[a,b], J.L. Bair[c,d], E.R. Homer[c*], P. Hosemann[a,e*]

[a] Nuclear Engineering Department, University of California-Berkeley, Berkeley, CA, USA

[b] Material Science and Technology Division, Los Alamos National Laboratory, Los Alamos, NM, USA

[c] Department of Mechanical Engineering, Brigham Young University, Provo, UT, USA

[d] Predictive Chemical and Nuclear Simulations, Pacific Northwest National Laboratory, Richland, WA, USA

[e] Material Science Division, Lawrence Berkeley National Laboratory, Berkeley, CA, USA

Corresponding Authors: P. Hosemann: peterh@berkeley.edu; E.R Homer:eric.homer@byu.edu

Abstract: The deformation of materials at cryogenic temperature is of interest for space, arctic and fundamental science applications. In this manuscript, a custom-built cooling system attached to a commercial picoindenter is used for *in-situ* cryogenic microcompression testing of Equal Channel Angular Pressed copper with real time electron backscatter diffraction. Stress-driven grain growth at cryogenic temperatures is observed during a series of elastic and plastic deformations. These results provide direct evidence for the previously predicted phenomenon, whereas previous ex-situ examinations demonstrated coarsening after cryogenic loading, but samples were not maintained at cryogenic temperatures between deformation and characterization.

KEYWORDS: Microcompression, Electron Backscatter Diffraction (EBSD), Cryogenic Temperatures, Stress-Driven Grain Growth

INTRODUCTION

Grain growth is an important mechanism for microstructural evolution, most often observed to occur at elevated temperatures where the thermal energy facilitates diffusive boundary migration [1, 2]. Stress has been demonstrated as a driving force to bias grain growth under conditions where thermal energy would be insufficient [3], with significant interest in this phenomenon in recent years [4-7].

Zhang et al. and Brons et al. demonstrated in ex-situ experiments that stress-driven coarsening may occur even at cryogenic temperatures [8-11]. Zhang et al. performed ambient and cryogenic indentation of nanocrystalline copper, followed by ambient temperature ex-situ characterization with a transmission electron microscope (TEM) of both samples; interestingly, the observed coarsening was more dramatic for the sample indented at cryogenic temperatures [9, 10]. Brons et al. followed this work with similar ex-situ indentation and characterization and demonstrated that the coarsening of different textures is correlated with the relative increase or decrease of specific grain boundary types; $\langle 100 \rangle$ nanotwinned Cu experienced an increase in Σ3 and Σ5 boundary content while the $\langle 111 \rangle$ nanotwinned Cu revealed a modest decrease in Σ3 content [8, 11].

Unfortunately, the ex-situ nature of the experiments leaves some question about when the coarsening occurred. It could have occurred at the cryogenic temperatures, which is supported by the decrease in the indentation load at cryogenic temperatures [9, 10]. But, it is also possible that the cryogenic temperatures simply prevented dynamic grain coarsening and encouraged the retention of the deformation energy in the system. As a result, coarsening could have occurred once the samples returned to ambient temperatures. Therefore, direct evidence of grain growth during deformation at cryogenic temperatures is still missing. The work presented here fills this gap and allows for direct proof of the phenomenon.

Here we use a custom-built, in-situ, cryogenic, picoindenter system for a scanning electron microscope (SEM). Furthermore, the system also has orientation imaging microscopy to index electron backscatter diffraction (EBSD) patterns to characterize the microstructural evolution. The system is a natural evolution of instrumented indentation with load and depth sensing [12, 13] that has ignited significant micro and nano scale mechanical testing across a wide array of applications [14,15] and material properties [16-18]. *In-situ* capabilities provide the ability to watch the deformation of the micro or nano scale specimen in real time, and also provide atmospheric control through the vacuum of the microscope. Cryogenic in-situ micromechanical testing is a more recent capability, with only a handful of custom-built systems available [19-23].

In this work we demonstrate, through the use of *in-situ* cryogenic experiments, that stress-driven grain coarsening actually can occur at cryogenic temperatures. The phenomenon is demonstrated in Equal Channel Angular Pressed (ECAP) copper tested on the in-situ system described. The in-situ system allows real

time EBSD of the microcompression specimen before, during, and after testing to examine the microstructural evolution. The following sections detail the setup of the in-situ system as well as the experiments, their results, and a discussion of the system and results.

EXPERIMENTAL

The material used in this investigation is ECAP, ultra-high purity, ultrafine grained copper, which has 15% 50–200 nm dislocation free grains, 37% 100–200 nm grains with chaotically distributed dislocations, and 48% 100–500 nm grains with sub-boundaries [24]. The ECAP copper is chosen for this work due to its ultrafine grain structure that (i) permits a larger number of grains in a micro-scale compression test [24] and (ii) allows for multiple grains to be present on the surface for EBSD characterization. The ECAP material originates from a 25 mm diameter rod. The severe plastic deformation processing involves pressing a copper billet through a 90° die 8 times while rotating the billet 90° after every other deformation pass. A full description of the processing can be found in [24] and is often described as route Bc in the ECAP literature.

The microcompression specimens of the ECAP copper are milled in a FEI FEG Quanta scanning electron microscope/focused ion beam dual beam (SEM/FIB) instrument at the University of California, Berkeley. The milling was performed with the sample on a 45° holder, which allows for milling perpendicular into two surfaces of the corner of the sample. The rough trenching of the pillars is completed with 7-15 nA and the final cleaning is performed with 0.5-1 nA. The final milled microcompression specimens have dimensions of ~2 x 2 x 5 μm and finished micro compression specimens can be seen in Figure 1A.

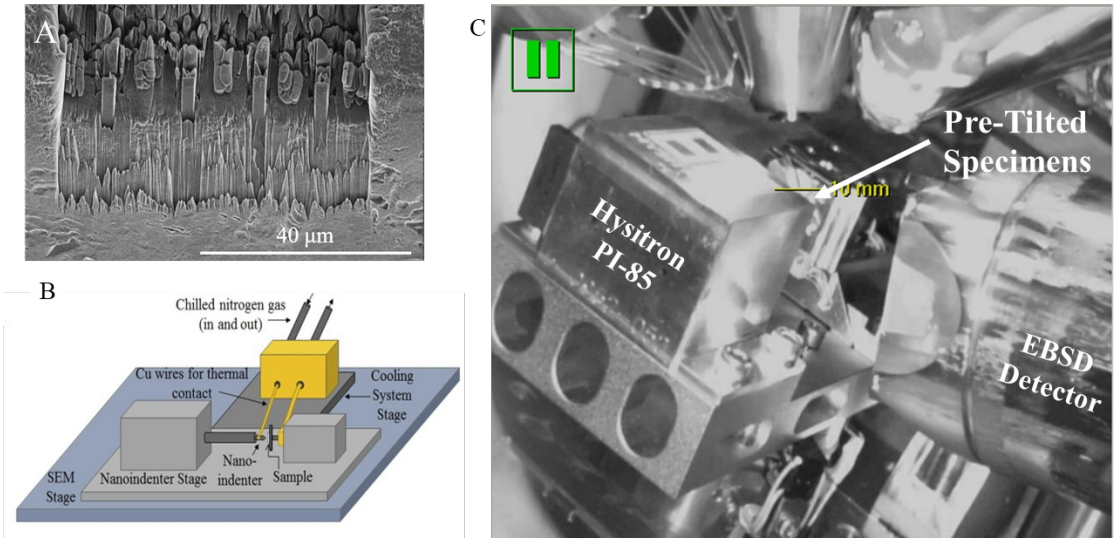

Figure 1: A) SEM image of the ECAP copper microcompression specimens before testing. B) Diagram illustrating cooling stage for the PI-85 system [23]. C) Infrared image of SEM/FIB chamber with EBSD camera inserted.

The ECAP copper microcompression specimens are mounted in a modified Hysitron PI-85 system for cryogenic testing. A custom-built cryogenic cooling system was manufactured by Hummingbird Scientific for use in conjunction with the Hysitron PI-85 nanoindenter (Figure 1B) [23]. The cryogenic system cools the tip and sample simultaneously in order to minimize thermal drift. The cooling data and system stability can be seen in [23]. A flatpunch conical diamond tip with a diameter of 5 µm is used for the microcompression tests. It is necessary to perform these tests under vacuum and good environmental control since ice will form on the tip and specimen from the air humidity, something that has been a major hurtle to development of cryogenic nanoindentation systems.

The microcompression specimens are mounted in the PI-85 at a 35-45º angle, as seen in Figure 1C, so EBSD patterns can be obtained. The PI-85 is then loaded into the instrument with the cooling stage on the opposite side of the Oxford EBSD detector with the Aztec software and analyzed using channel 5 software.

Once the chamber is pumped to a vacuum, the whole PI-85 set up, with the ECAP copper specimens and cooling stage, is tilted 25-35°. The “pre-tilt” loading of the sample plus the additional tilt in the SEM/FIB enables the face of the microcompression specimens to be ~70° from the SEM beam, which is the optimal angle for EBSD measurements. It should be noted that the specimens may not have been at exactly 70°, leading to some uncertainty in the absolute orientations; however, the interest is in the relative orientations of the grains, which gives us the grain boundary character, as well as the evolution of the microstructure. Pre-testing EBSD maps at room temperature are taken to verify geometry and function of all components prior to cooling the specimen. Subsequently the specimen is cooled to cryogenic temperature using chilled nitrogen gas flowing through a heat exchanger in liquid nitrogen. After the specimen reaches thermal equilibrium (138 K) with the cooling block, additional EBSD scans at cryogenic temperature are taken to verify the systems function and pre-experimental condition. The testing of the microcompression specimens is performed using the load-controlled mode on the PI-85. Since the investigation of this work is to evaluate stress-driven grain coarsening at cryogenic temperature, the microcompression specimens are loaded in both the plastic and elastic regime before a final plastic deformation test; the experimental literature on the stress-driven grain coarsening at cryogenic temperature is from plastic deformation [8-11]. Figure 2a shows the planned schedule for the loading and temperature. The schedule consists of a large plastic load, followed by several elastic loadings of 400 µN, and a final plastic load. The 400 µN elastic loads correspond to a stress of ~82 MPa in the microcompression specimen, which is well below the yield stress of 383 ± 34 MPa from a room temperature microcompression testing [24]. Each elastic loading is held for 300 seconds at the peak load and then a posttest EBSD scan is performed. The final

plastic deformation test is terminated early enough to still have a suitable surface for EBSD posttest. After all of the microcompression specimen tests the sample and tip of the PI-85 are heated back to room temperature.

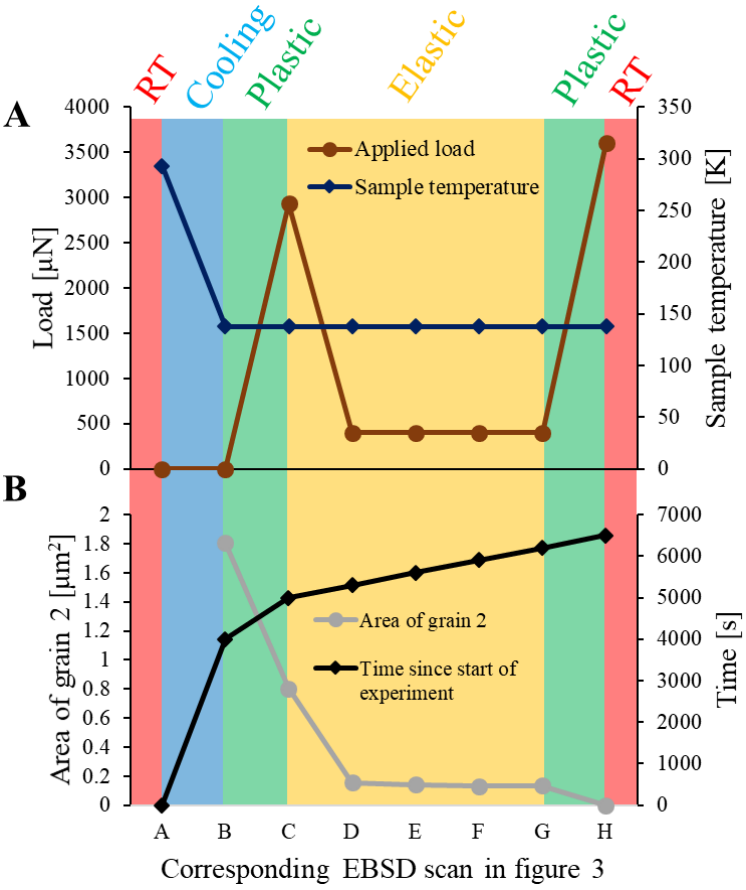

Figure 2: Graph showing the correspondence between load, temperature, grain 2 area, and time for various test states, including EBSD snapshots similarly identified in Figure 3. The microcompression specimen is cooled from RT (red) to cryogenic temperatures (blue), which takes ~1 hour for cooling and thermal stabilization. Loading includes: initial plastic loading (green), where the specimen yields around 2800 μN; 4 elastic loads (yellow), each at 400 μN; and final plastic load (green). Specimen is then returned to RT.

RESULTS AND DISCUSSION

Figure 2a shows the planned and executed schedule for loading and temperature. Figure 3 shows the pre and posttest EBSD maps of a small region of the pillar corresponding to the load/temperature schedule in Figure 2. The approximate pillar outline and orientation are outlined in Figure 3a. Unindexed pixels in the pillar region primarily occur at grain boundaries and from progressive deformation, both

of which cause signal degradation and make accurate determination of orientation difficult.

The plastic loading causes significant changes to the microstructure, as can be seen in Figures 3b and 3c. The most dramatic change occurs in the brown grain, labeled as grain 2 in Figure 3a. Figure 3b shows the change of the grain area for grain 2, which experiences a 55% reduction in area during the plastic loading; grain areas are calculated using ImageJ. The misorientations between the grains in Figure 3a are given in Table 1. It appears that grain 2 is embedded inside grain 1, where the boundary between them has a misorientation of ~6.4°, indicating that it is a low-angle grain boundary. It should be noted that a threshold of 4° is used to determine when a change in orientation is sufficient to be identified as a grain boundary in the orientation maps.

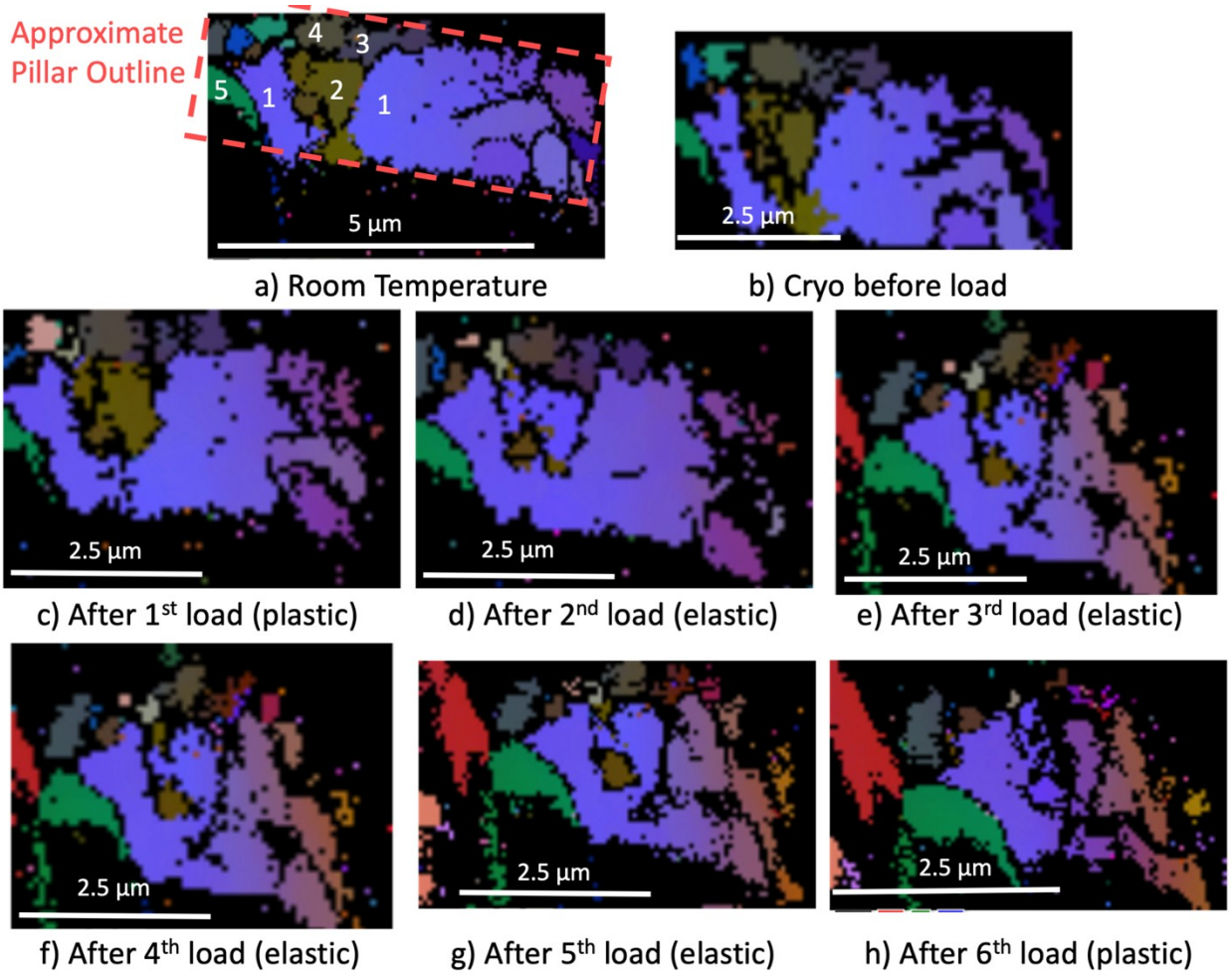

Figure 3: Grain maps at each step illustrated in Figure 2. Grain 2 contracts significantly between (b) and (c), between (c) and (d), and again between (g) and (h). Scale bar change between room and cryogenic temperature (a and b) results from need to re-center the specimen after cooling caused shrinkage.

Table *1*: Boundary information for all grains labeled in Figure 3a, including misorientation angle, axis of rotation, and offset angle of actual axis of rotation from integer axis of rotation listed.

Grain Boundary	Misorientation	Axis of Rotation	Offset
1-2	6.4°	$[23\acute{1}]$	3.42°
1-3	22.5°	$[340]$	3.61°
2-3	12.5°	$[\acute{3}\acute{4}\acute{1}]$	3.12°
2-4	10°	$[\acute{1}\acute{2}0]$	5.57°
3-4	6.7°	$[320]$	4.66°
1-5	56.6°$(\Sigma 3)$	$[\acute{1}\acute{1}1]$	3.13°

The results of the series of elastic loads and holds can be seen in Figures 3d-3g. The first elastic load causes significant reduction to grain 2, resulting in a further 80.7% reduction; indicating that both elastic and plastic loading is sufficient to cause the microstructural coarsening. However, the remaining elastic loads appear to cause very little additional change, as indicated by the snapshots in Figure 3 and the grain area in Figure 2b. The final plastic loading causes grain 2 to almost completely disappears; a small patch of grain 2 remains at the top of Figure 3h but it is not included in the area calculations in Figure 2b.

The in-situ cryogenic microcompression tests provide clear evidence of microstructural coarsening. While there are a variety of factors that could, or would have been expected to, play a role here, we discuss a few of the most relevant.

It is interesting to note that the grain that shrinks the most, grain 2, is surrounded on most sides by a low-angle grain boundary. The presence of this low-angle grain boundary is confirmed in the local misorientation map in Figure 4a. Furthermore, Figure 4b demonstrates that the region previously occupied by grain 2 has low magnitudes of local misorientation changes. This is consistent with a recrystallizing grain consuming a deformed region, leaving behind a region with little deformation. It should be noted however, that unlike a recrystallization, the grain that grows is not free from deformation, except in the swept region, since the initial material is heavily deformed ECAP copper.

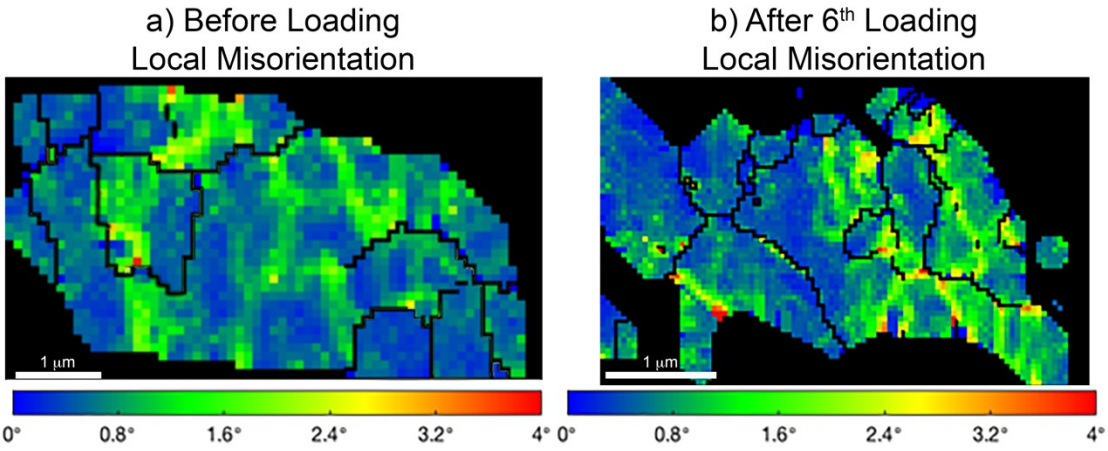

Figure 4: Local misorientation changes before and after applied load demonstrates changes caused by the boundary motion.

This observation begs the question of whether the boundary migration is driven by the inherent mobility of the boundary, the deformation structure, or disparate grain sizes. Simulations of grain boundary migration suggest that specific boundaries are likely to be mobile at cryogenic temperatures, like Σ3, Σ7, Σ9, and Σ11 CSL boundaries [25-31]. Unfortunately, simulations have not examined the cryogenic mobility of low-angle grain boundaries, like the one that consumes grain 2. However, Brons et al. note that low-angle boundaries can experience significant evolution in cryogenic indentation, depending upon the location relative to the indentation [8]. Furthermore, Brons et al. also find that some of these same CSL boundaries are involved with the cryogenic coarsening [6]. Thus, there is some indication that specific boundaries might have inherent mobilities that facilitate cryogenic coarsening.

On the other hand, room temperature in-situ, X-ray Laue diffraction microscopy examining the 3D migration of a recrystallizing boundary suggest a different conclusion [32]. In that work, certain facets of a recrystallizing boundary migrate, while other facets do not. Together with accompanying simulations of the same boundaries, except without a deformed structure [33], the results indicate that the nature of the deformation microstructure plays a bigger role in the migration of the recrystallizing boundary than the inherent mobilities of the boundaries in question.

This is possibly supported by the fact that the one Σ3 CSL boundary in the present sample doesn’t migrate. Simulations indicate that most Σ3 boundary plane orientations, excluding the coherent twin plane, are expected to be mobile at cryogenic temperatures [27]. Without the full 5D characterization (misorientation and boundary plane orientation) of the boundaries, one cannot definitively say whether the Σ3 CSL boundary in the present sample would have been expected to be mobile.

This could also be the result of abnormal grain growth. The grains in question have grain sizes much larger than the original grain size of the sample (grain 2 is ~1.5 microns wide while grain 1 is ~5 microns wide, both of which are much larger than the ~200 nm grain size). Perhaps this abnormally large grain will consume its surrounding neighbors regardless of their nature, as routinely observed in abnormal grain growth. On the other hand, grain 1 appears to preferentially consume grain 2, and not all other surrounding grains, though this is difficult to see with the collected data.

Thus, while the present work shows clear evidence for stress-driven microstructural coarsening at cryogenic temperatures, the underlying cause of the coarsening requires further investigation. Furthermore, the grain size and deformed nature of the present sample [24] differ from the undeformed and fine structures of the previous studies [8-11], such that the mechanism and/or driving force for the coarsening could be different.

It should also be noted that while the *in-situ* SEM testing makes this observation possible, and removes some of the challenges of the *ex-situ* testing, it is not without challenges. In particular, there could be gallium contamination of the microcompression sample from the manufacturing. Gallium implanted during the milling could inhibit or prevent the hypothesized cryogenic migration behaviors. Also, it could be possible that the loading conditions in this test were insufficient to induce the hypothesized migration behaviors in the other grain boundaries.

CONCLUSION

In the present work, for the first time *in-situ* SEM cryogenic testing of samples on the micro scale with real time microstructure characterization has observed cryogenic stress-driven grain coarsening. The observed phenomena is direct proof that was previously hypothesized [8-11]. The setup utilized here allows the microstructure to be characterized following several loading cycles, ensuring that all changes that occur do so at cryogenic temperatures, and not during any subsequent processing for posttest characterization. The major microstructural coarsening involves a low-angle grain boundary. The cause of the boundary migration could be dominated by the inherent mobility of the boundary and that it could be dominated by the underlying deformation microstructure. This work proofs that grain growth can occur at cryostatic temperatures on ultrafine grained and nanograined materials.

ACKNOWLEDGEMENTS

The authors would like to acknowledge Daniel Kiener from the Erich Schmidt Institute in Austria and Brad Boyce from Sandia National Laboratory for encouraging discussion on this topic.

FUNDING

Research supported as part of FUTURE (Fundamental Understanding of Transport Under Reactor Extremes), an Energy Frontier Research Center funded by the U.S. Department of Energy (DOE), Office of Science, Basic Energy Sciences (BES) (neutron scattering studies) and by the U.S. Department of Energy (DOE), Office of Science, Basic Energy Sciences (BES) under Award #DE-SC0016441.

REFERENCES

[1] A.P. Sutton, R.W. Balluffi, *Interfaces in Crystalline Materials,* Oxford University Press (1995)

[2] G. Gottstein, L.S. Shvindlerman, *Grain boundary migration in metals: thermodynamics, kinetics, applications,* Second Edition Taylor & Francis Group Press (2010)

[3] D.W. Bainbridge, H.L. Choh, E. H Edwards, *Acta Metall Mater*. 2 322 (1954) doi:10.1016/0001-6160(54)90175-3

[4] J.F. Panzarino, Z. Pan, T.J. Rupert, *Acta Materialia* 120 (2016)

[5] T.J. Rupert, D.S. Gianola, Y. Gan, K.J. Hemker, *Science* 326 (2009)

[6] C.V. Thompson, R. Carel, *J. Mech. Phys. Solids.* 44 (1996)

[7] J.A. Sharon, P-C Su, F.B. Prinz, K.J Hemker, *Scripta Mater.* 64 (2011)

[8] J.G. Borns, J.A. Hardwick, H.A. Padilla II, K. Hattar, G.B. Thompson, B.L. Boyce, *Mater. Sci. Eng. A* 592 182 (2014)

[9] K. Zhang, J.R. Weertman, J.A. Eastman, *Appl. Phys. Letters* 87 (2005)

[10] K. Zhang, J.R. Weertman, J.A. Eastman, *Appl. Phys. Letters* 85 (2004)

[11] J.G. Brons, H.A. Padilla II, G.B. Thompson, B.L. Boyce, *Scripta Mater.* 68 (2013)

[12] J.L. Loubet, J.M. Georges, O. Marchesini, G. Meille, *J. Tribology* 106 43 (1984)

[13] D. Newey, M.A. Wilkens, H.M. Pollock, *J. Phys*. 15 119 (1982)

[14] X. Li, B. Bhushn, *Mater. Character.* 48 (2002)

[15] S.J. Bull, *J. Phys. D: Appl. Phys.* 38 (2005)

[16] M.D. Uchic, D.M. Dimiduk, J.N. Florando, W.D. Nix, *Science* 305, (2004)

[17] P. Hosemann, *Scripta Mater.* 143 (2018)

[18] M.D. Abad, S. Parker, D. Frazer, M. Rebelo de Figueiredo, A. Lupinacci, K. Kikuchi, P. Hosemann, *Oxid. Met.* 84 211 (2015)

[19] B.D. Snartland, A.B. Hagen, C. Thaulow, *Eng. Fract. Mechan.* 175 (2017)

[20] S-W Lee, Y.T. Cheng, I. Ryu, J.R. Greer, *Sic. China Tech. Sci* 57 (2014)

[21] A.B. Hagen, C. Thaulow*, Mater. Sci. Eng. A* 678 (2016)
[22] S-W Lee, L. Meza, J.R. Greer, *Appl. Phys. Letters* 103 (2013)
[23] A. Lupinacci, J. Kacher, A. Eilenberg, A.A. Shapiro, P. Hosemann, A.M. Minor, *Acta Mater.* 78 56 (2014)
[24] C. Howard, D. Frazer, A. Lupinacci, S. Parker, R.Z. Valiev, C. Shin, B.W. Choi, P. Hosemann, *Mater. Sci. Eng. A* 649 104 (2016)
[25] J.L. Bair, E.R. Homer, *Acta Mater.* 162 (2019)
[26] J.L. Priedeman, D.L. Olmsted, E.R. Homer, *Acta Mater.* 131 553 (2017)
[27] J. Humberson, E.A. Holm, https://arxiv.org/abs/1704.03088
[28] D.L. Olmsted, E.A. Holm, S.M. Foiles, *Acta Mater.* 573 704 (2009)
[29] E.R. Homer, E.A. Holm, S.M. Foiles, D.L. Olmsted*, JOM* 66 114 (2014)
[30] E.R. Homer, S. Patala, J.L. Priedeman, *Sci. Rep.* 515 (2015)
[31] J. Humberson, E.A. Holm, *Scripta Mater.* 130 1 (2017)
[32] Y.B. Zhang, J.D. Budai, J.Z. Tischler, W. Liu, R. Xu, E.R. Homer, A. Godfrey, D. Juul Jensen, *Scientific Reports* 7 (2017)
[33] E.R. Homer, 36th Riso International Symposium on Materials Science, IOP Publishing, Roskilde, 2015: p. 012006.

Figure and Table Captions

Figure 1: A) SEM image of the ECAP copper microcompression specimens before testing. B) Diagram illustrating cooling stage for the PI-85 system [23]. C) Infrared image of SEM/FIB chamber with EBSD camera inserted.

Figure 2: Graph showing the correspondence between load, temperature, grain 2 area, and time for various test states, including EBSD snapshots similarly identified in Figure 3. The microcompression specimen is cooled from RT (red) to cryogenic temperatures (blue), which takes ~1 hour for cooling and thermal stabilization. Loading includes: initial plastic loading (green), where the specimen yields around 2800 μN; 4 elastic loads (yellow), each at 400 μN; and final plastic load (green). Specimen is then returned to RT.

Figure 3: Grain maps at each step illustrated in Figure 2. Grain 2 contracts significantly between (b) and (c), between (c) and (d), and again between (g) and (h). Scale bar change between room and cryogenic temperature (a and b) results from need to re-center the specimen after cooling caused shrinkage.

Figure 4: Local misorientation changes before and after applied load demonstrates changes caused by the boundary motion.

Table *2*: Boundary information for all grains labeled in Figure 3a, including misorientation angle, axis of rotation, and offset angle of actual axis of rotation from integer axis of rotation listed.